



Review

Tracing the Pathways of Waters and Protons in Photosystem II and Cytochrome c Oxidase

Divya Kaur ^{1,2,†}, Xiuhong Cai ^{1,3,†}, Umesh Khaniya ^{1,3}, Yingying Zhang ^{1,3}, Junjun Mao ¹, Manoj Mandal ¹ and Marilyn R. Gunner ^{1,2,3,*}

¹ Department of Physics, City College of New York, New York, NY 10031, USA; dmatta@gradcenter.cuny.edu (D.K.); xcai@gradcenter.cuny.edu (X.C.); ukhaniya@gradcenter.cuny.edu (U.K.); yzhang5@gradcenter.cuny.edu (Y.Z.); jmiao@ccny.cuny.edu (J.M.); mandalmanojcu@gmail.com (M.M.)

² Ph.D. Program in Chemistry, The Graduate Center of the City University of New York, New York, NY 10016, USA

³ Ph.D. Program in Physics, The Graduate Center of the City University of New York, New York, NY 10016, USA

* Correspondence: mgunner@ccny.cuny.edu

† The first two authors contributed equally to this paper.

Received: 1 January 2019; Accepted: 28 January 2019; Published: 31 January 2019



Abstract: Photosystem II (PSII) uses water as the terminal electron donor, producing oxygen in the Mn_4CaO_5 oxygen evolving complex (OEC), while cytochrome c oxidase (CcO) reduces O_2 to water in its heme–Cu binuclear center (BNC). Each protein is oriented in the membrane to add to the proton gradient. The OEC, which releases protons, is located near the P-side (positive, at low-pH) of the membrane. In contrast, the BNC is in the middle of CcO, so the protons needed for O_2 reduction must be transferred from the N-side (negative, at high pH). In addition, CcO pumps protons from N- to P-side, coupled to the O_2 reduction chemistry, to store additional energy. Thus, proton transfers are directly coupled to the OEC and BNC redox chemistry, as well as needed for CcO proton pumping. The simulations that study the changes in proton affinity of the redox active sites and the surrounding protein at different states of the reaction cycle, as well as the changes in hydration that modulate proton transfer paths, are described.

Keywords: proton pumping; network analysis; proton affinity; proton coupled electron transfer

1. Introduction

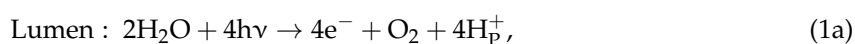
The proton coupled electron transfer reactions that take place in the membranes of photosynthetic and aerobic organisms generate the transmembrane electrochemical gradient used to fuel ATP synthesis and other metabolic processes. Photosystem II (PSII) uses the energy of light and cytochrome c oxidase (CcO) the energy released transferring electrons from cytochrome c to O_2 , to add to the proton gradient [1–3]. In PSII, the reduced quinone product retains enough energy to drive proton transfer catalyzed by complex III (the bc_1 or b_6f complexes), while CcO is the terminal redox acceptor, producing water as the end product of aerobic metabolism. Each of these proteins carries out proton coupled electron transfers, where the substrate changes protonation state as it undergoes redox chemistry. In addition, CcO also transfers protons across the membrane embedded protein from the N-side (negative side, high pH) to the P-side (positive side, low pH).

Water is a key constituent in PSII and CcO. Water is the substrate for PSII and product for CcO. Internal waters stabilize buried ionized groups and water pathways permit proton transfer between the surface and the protein interior. Thus, the reaction can be controlled by changing hydration levels through the reaction cycle. With the elucidation of the structures of these proteins, computational

simulations have made it possible to begin to understand the mechanism in atomic detail. Our focus will be on the simulation techniques that provide insight into the thermodynamics of electron and proton transfer reactions at buried sites in proteins and on the identification of essential pathways for protons and waters.

1.1. Photosystem II

Cyanobacteria, algae, and higher plants carry out oxygenic photosynthesis [1]. PSII uses water as the terminal electron donor, leading to the release of O₂ as a byproduct [4–6]. Within PSII, light activation leads to the oxidation of the redox active chlorophylls, P₆₈₀, to P₆₈₀⁺ and electron transfer across the protein leads to reduction of plastoquinone (Q) to plastoquinol (QH₂). Oxidation of water takes place at the oxygen evolving complex (OEC), a Mn₄CaO₅ cluster. The redox active tyrosine, Y_Z, is the intermediate redox cofactor, reducing P₆₈₀⁺, and in turn being reduced by the OEC [7]. The OEC is located near the lumen (P-side) of PSII so that vectorial electron transfer adds to the proton gradient across the thylakoid membrane without protons transferring across the membrane [2]. The overall reaction is



Protons (H_P⁺), are lost from water to the P-side while Q binds protons (H_N⁺) from the N-side (stroma). Thus, Q reduction and water oxidation both add to the pH gradient. Overall, the transmembrane ΔpH is increased by 1 proton/electron. Figure 1a shows a schematic picture of the PSII mechanism.

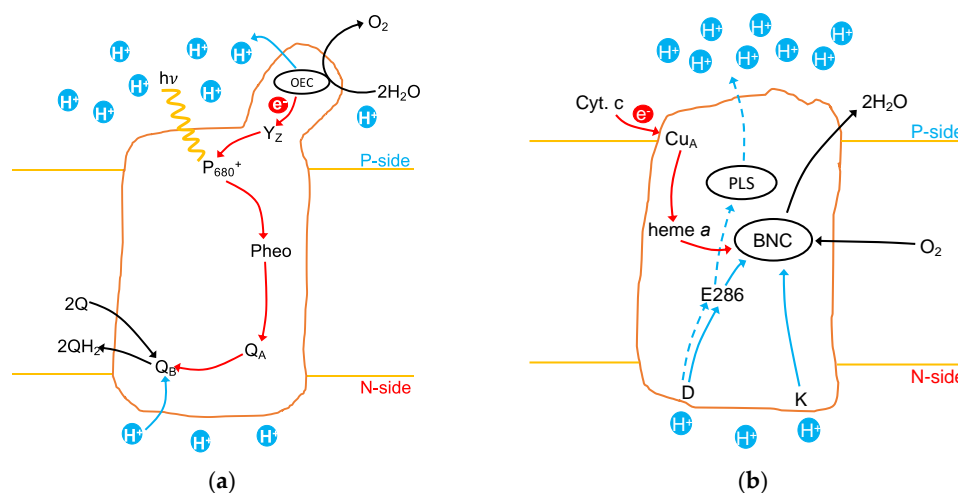


Figure 1. Schematic illustration of PSII and CcO showing key features of each mechanism. Red lines: electron transfer pathways; solid blue lines: chemical transfer pathways; dashed blue lines: pathways for pumped protons; black lines: substrate and product pathways. (a) In PSII the excited P₆₈₀⁺, transfers an electron via a pheophytin (Pheo) and plastoquinone (Q_A) to a second plastoquinone (Q_B). Following a second turnover, the doubly reduced Q_B has bound two protons from the N-side and dissociated into the membrane as QH₂. The active site oxygen evolving complex (OEC) comprised of four Mn, five μ-O and one Ca in a cubane structure with a dangling Mn. It reduces P₆₈₀⁺ via Y_Z. Following four turnovers, the OEC oxidizes H₂O to O₂ in the S₄ state, releasing four protons to the P-side of the membrane. (b) In CcO, the active site, BNC, consists of heme a₃ and Cu_B with the redox active Y288. Electrons are transferred from cytochrome c via Cu_A and heme a to the BNC. Following accumulation of four electrons, O₂ is bound to the BNC and reduced to H₂O. The four protons needed for chemistry are transferred from the N-side through the D- and K-channels. The four pumped protons enter through the D-channel and are transiently held in the proton loading site (PLS), located near the P-side of CcO, before being released to the P-side of the membrane. The D-channel ends at E286, which passes a proton to the BNC or PLS.

The OEC goes through five increasingly oxidized states (S_0 to S_4) losing four electrons [8,9] and generating a redox potential that is positive enough to oxidize water in the single step $S_4 \rightarrow S_0$ [10]. Much of the current research on the OEC focuses on producing a model of the S-state cycle that ends in O–O bond formation. Computational simulations [11,12] combined with XFEL structures [13,14] and many experiments [6] provide an emerging picture of the OEC structure through the S-state cycle and the mechanism by which the cluster can catalyze water oxidation. One question is how the OEC Mn cluster changes shape through the S-state cycle. Conventional crystal structures gave a glimpse [15], but the OEC becomes highly reduced (below S_0) under X-ray illumination [16,17]. Crystal structures obtained with X-ray free electron laser (XFEL) measurements provide a chance to obtain information about individual S-state structures [14,18–21]. However, the protein in the crystal is never in one state: with conventional X-ray crystallography it is in a mixture of highly reduced states [17]; dark adapted XFEL structures will be mostly in the S_1 state, but will contain some S_0 as well; with multi-flash spectroscopy the non-unity quantum yield means there will always be a mixture of states [14]. In addition, extracting structural information for lighter-atoms (like O) surrounded by electron-rich Mn is problematic [22]; and the structures do not provide the location of protons [23,24].

The OEC is made up of three Mn, one Ca, and five μ -oxo ligands held together in a cubane structure with a dangling Mn (Figure 2a). The combinatorics of a cluster with four Mn lead to 4 possible redox isomers for S_0 ($(\text{Mn}^{\text{III}})_3(\text{Mn}^{\text{IV}})_1$) with any of the four Mn being first oxidized, 12 combinations leading to S_1 ($(\text{Mn}^{\text{III}})_2(\text{Mn}^{\text{IV}})_2$), 4 for S_2 ($(\text{Mn}^{\text{III}})_1(\text{Mn}^{\text{IV}})_3$), and 1 for S_3 ($(\text{Mn}^{\text{IV}})_4$). S_4 removes an electron from a Mn or substrate oxygen [6,25]. Combined QM/MM analysis along with EXAFS and XRD measurements have established the redox isomer and atomic positions for S_0 [26], S_1 [27], S_2 [28,29], and S_3 [4,30–32] states. The low energy redox state for S_0 is 3433 (giving the oxidation states of the Mn designated 1 through 4) while S_1 is 3443 [33].

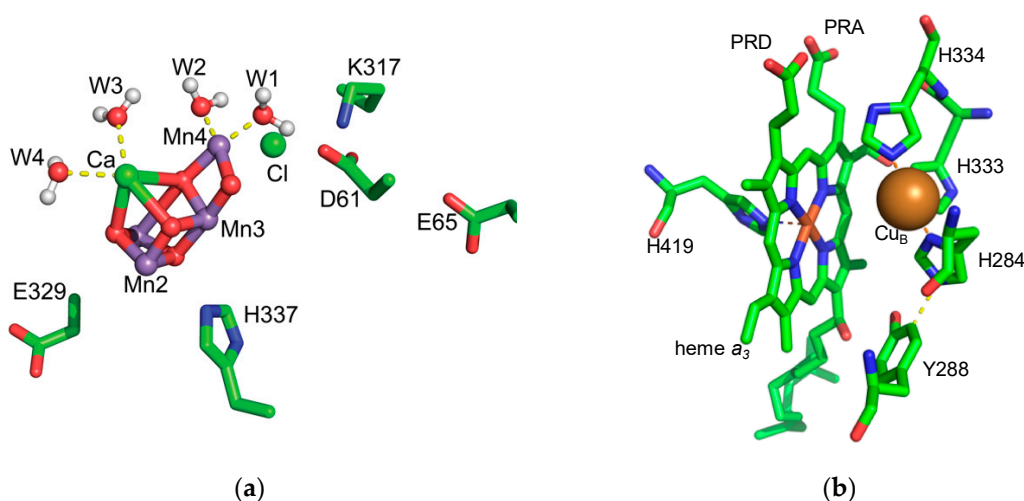


Figure 2. Structure of the active sites of PSII and CcO. (a) The Mn_4CaO_5 cluster of the OEC. The water ligands to Mn4 and Ca^{II} as well as the nearby residues D1-E329, D1-H337, D1-D61, D1-E65, D2-K317 and nearby Cl are shown. (b) The structure of the BNC in CcO. Cu_B is the sphere. Heme a_3 , Y288 as well as the ligands of heme a_3 and Cu_B are shown in sticks. Y288 is covalently bound to the Cu_B ligand H284, PRD and PRA are the propionate acids of heme a_3 and may be part of the PLS. Substrate water will bind between Cu_B and the central iron of Heme a_3 .

For S_2 , two redox isomers are found [29,33] as a result of Mn1 and Mn4 competing to make the bridging O5 their sixth ligand [29,34,35]. Model system studies [36] show Mn^{III} can have five or six ligands but an oxidized Mn^{IV} needs six. In the redox isomer where Mn4 is oxidized (3444) O5 moves towards the dangler Mn4 giving a $g = 2$ multiline EPR signal. In the other, Mn1 is oxidized (4443) and O5 completes its coordination shell, giving the $g = 4.1$ broad EPR signal [37].

S₃ [38] is primed for reaction. The growing agreement about the structure of this state comes from a dialog between QM/MM simulation and XFEL experiment [20,22,30,39–41]. In the S₃ state, a new water (or hydroxyl) is added. The two S₂ isomers can lead to an open state for S₃ where the added substrate O is bound to the dangling Mn4 or a closed state where the substrate is on Mn1. The incomplete ligand shells of Mn1 and Mn4 in states below S₃ may deny a position for the second substrate water to bind before S₃ [42–44].

There are four terminal waters in the OEC, two coordinated to Mn4 (W1, W2) and two at Ca^{II} (W3, W4) (Figure 2a). It is proposed that substrate water may be contributed by a ligand to Mn4 [4,41] or Ca^{II} [34,45], or it may arrive from a second shell water near O4 [31,41].

1.2. Cytochrome *c* Oxidase

CcO (complex IV) is the terminal protein of the respiratory electron transfer chain in mitochondria and aerobic bacteria, using the electrons from cytochrome *c* produced in complex III, to reduce O₂ to water [46–49]. CcO catalyzes the reaction that reverses the OEC chemistry, using the energy liberated in the reduction of O₂ to add to the transmembrane proton gradient. However, rather than using a Mn based cofactor, the active site binuclear center (BNC) of CcO contains a heme (heme *a*₃) and a copper (Cu_B) [50] (Figure 2b). While the OEC is near the P-side of the protein, the BNC is in the center so that substrate protons must move into the protein, from the N-side, to produce water. During one catalytic cycle, four electrons are transferred from cytochromes *c* bound at the P-side, to Cu_A, a bi-copper site, and then to a low-spin heme *a*, finally to the BNC [51]. Meanwhile, eight protons are taken up from the N-side, with four protons delivered to the BNC as needed for the oxygen chemistry (chemical protons), and four protons translocated across the membrane (pumped protons). The overall reaction is:



The reaction leads to two charges/electron translocated across the membrane. Figure 1b provides a schematic illustration of the CcO mechanism.

CcO cycles through four increasingly reduced states (denoted O, E, R, and P/F) [48,49,52]. The P state occurs following reduction of O₂. P and F [53] have the same number of electrons, while F has bound another proton. As with the OEC where water oxidation is carried out in the S₄→S₀ step, CcO carries out the full reduction of O₂ in one step (R→P) to minimize the production of reactive oxygen species [51]. Heme *a* is the electron donor to the BNC, analogous to the relationship of Y_z to the OEC. At each redox state transition, one electron and one chemical proton is sequentially added to the BNC to help ensure redox leveling. As in the OEC where the second water is not added until late in the reaction cycle (in S₃), O₂ is only bound when the BNC is in the fully reduced, R, state (Fe^{II}_{a3}, Cu^I_B, Y–OH). The ensuing reaction then oxidizes the BNC and reduces O₂ to form the P state (Fe^{IV}_{a3} = O[−], Cu^{II}_B–OH[−], YO[•]). Thus, the bound O₂ accepts four electrons, two from the feryl heme *a*₃, one from Cu_B, and the fourth from a tyrosine covalently bonded to one of the three histidine ligands of Cu_B. This yields the P_M state [54]. O₂ reduction can alternatively pass through the P_R state (Fe^{IV}_{a3} = O[−], Cu^{II}_B–OH[−], Y–O[−]) when the reduced heme *a* rather than the tyrosine contributes an electron to the reaction [55]. The subsequent reduction of the BNC is coupled to the addition of protons to the oxygen bound to heme *a*₃ and Cu_B, which are released as water [53,56,57]. The currently accepted order of proton and electron additions is F: (Fe^{IV}_{a3} = O^{2−}, Cu^{II}_B, Y–O[−]) to O: (Fe^{III}_{a3}–OH[−], Cu^{II}_B, Y–O[−]), to E: (Fe^{III}_{a3}–OH[−], Cu^I_B, Y–OH), and to R: (Fe^{II}_{a3}, Cu^I_B, Y–OH). The catalytic cycle of CcO has been established by DFT simulation combined with many experiments [51,53,58–60].

2. Finding the Protons in the Active Site and the Surrounding Protein

PSII and CcO both carry out multielectron chemistry, where a series of single electron transfers create a sequence of redox intermediate states. The loss or gain of electrons is coupled to the loss or gain of protons [61]. The order of oxidation of the four OEC Mn or the BNC heme *a*₃ and Cu_B reflects

both the relative redox potential of each site as well as the proton affinity of the different protonatable groups in the cluster. Protonation changes of products or substrates (chemical protons) are driven by large changes in proton affinity due to oxidation or reduction of the Oxo-Mn [62–64] or heme-Cu redox cofactors [65].

In addition, there are many buried acidic and basic amino acids in the protein surrounding the various redox active sites. The charge state of these residues can modulate the electrostatic potential, tuning the OEC and BNC electron and proton affinity. These residues may change protonation states in response to changes at the active site. The proton transfer pathways to buried sites also require buried groups that can transiently change protonation state. The protonation and tautomer state of both the active site and the protein is often experimentally elusive, yet the thermodynamic analysis of the redox cycle relies on establishing the correct states for many sites in the protein and cofactor. In addition, any molecular dynamics (MD) or QM/MM simulation must make a best guess as to which groups are protonated to start the calculation. There are several simulation techniques that can help establish the likely protonation or tautomer states by the analysis of the proton affinity of the cofactor and protein in each redox intermediate state [66–69].

2.1. Methods of Calculation

An acidic or basic residue can be in its protonated or deprotonated form and each redox cofactor has a defined oxidation state. A microstate of the protein will define the protonation state of each residue and the redox state of each cofactor. If each of the n groups of interest has m protonation or redox states, there are m^n microstates. In the calculation of Boltzmann distribution of protonation states within the protein, it is generally assumed that each intermediate in the redox cycle finds the lowest energy protonation states and redox state isomers and that the protonation state of the surrounding protein can come to equilibrium with the redox changes within microseconds. There are a variety of methods to determine the relative free energy of the possible redox and protonation microstates [66,67]. The different simulation methods differ in the level of theory used, the elements that are fixed or allowed to change and the region of the protein that is included in the simulation. The key methods that help to establish the redox and protonation equilibria distributions are QM based calculations (DFT and QM/MM), CE/MC methods that use Monte Carlo (MC) sampling with continuum electrostatics (CE) energies and constant pH molecular dynamics (cpHMD). These methods are distinct from conventional molecular dynamics (MD) calculations, as these must fix the chemical form of the protein and cofactors.

Monte Carlo approaches that use classical CE energies allow the sampling of multiple redox states and many protonatable groups in the whole protein [66]. The programs MCCE [70] and Karlsberg [71] use this approach. These methods do not calculate E_m s or pK_a s from first principles. Rather a known titration of an analog of the residue in water provides a reference energy [64,65,72]. The calculations then determine how interactions within the protein modulate the energy, shifting the electron and proton affinity. Assuming we have a good value for the interaction energy between all pairs of charges, the equilibrium distribution of protonatable residues and redox active cofactors is determined via Monte Carlo sampling. The resulting Boltzmann distribution at a given pH and E_h can have groups with a non-integer probability of being protonated or reduced as would be found in experiment near the pK_a or E_m . The use of Grand Canonical Monte Carlo (GCMC) methods allows the binding or release of functionally important ions, such as chloride, and of explicit waters in the same analysis that determines the distribution of ionization states.

One strength of CE/MC methods is that they can reliably converge to the equilibrium distribution for the whole protein. It can be relatively straightforward to interrogate the outcome to determine the contribution of individual residues to the result. A strength and weakness of the CE method is the use of a dielectric constant. This accounts for the different polarization of the protein, water, and lipid that screens interactions, so provides an inexpensive polarizable force field. However, the value of the dielectric constant is an ongoing subject of dispute [66]. CE methods can only include the influence of

quantum effects such as changing spin state or of Jahn–Teller effects by having access to values for E_m s and pK_a s of closely related reference reactions. It is also difficult to incorporate protein motion into the calculation because MC sampling is far more efficient with a fixed protein backbone. The calculations may allow side chain rotamer sampling [69,70]. A current work-around to the fixed backbone is to average the charge state distributions calculated in multiple snapshots from MD simulation or from multiple crystal structures, which provide a distribution of likely conformations. One problem is that an MD simulation will always seek to stabilize the charge states assigned to the simulation [73,74].

The goal is to analyze the free energy of different mixtures of protonation and redox states while the protein samples conformational space. Constant pH MD (cpHMD) is an emerging technique which may be able to accomplish this goal [75–80]. One method is to run MD for a short time and then exit and use MC to determine the equilibrium protonation state and then resume the MD trajectory. While this method has significant promise, it has serious barriers to its application to the large proteins of interest here. Each addition or removal of a charge from the protein in a MC step creates a major disturbance for the system when resuming MD, requiring re-equilibration after each move. This process is quite difficult to converge, especially for the proteins of interest here where many sites have closely coupled changes in ionization states. In addition, the classical MD portion of the simulation uses Coulomb's law in vacuum, which can overestimate the electrostatic interactions [81]. As the key questions involve the interactions of buried charges the uncertainty of the electrostatic energy may be addressed by use of polarizable force fields. Unfortunately, this adds significant computational cost [80].

Consideration of the OEC and BNC requires analysis of multi-electron processes in biometallic complexes [82]. Simple classical methods cannot account for the changes in electron distribution, spin states, polarization, and cluster geometry that accompany the reactions. These elements require a quantum mechanical (QM) approach. To permit the calculations to include sufficient number of atoms DFT [83] and other semi-empirical [84] methods are used. The accuracy and computational cost of all QM calculations also depend on the basis set used. QM/MM (quantum mechanical and molecular mechanical) approaches allow the effects of the surrounding protein to be included [85]. All of these QM based methods calculate the optimized geometry and total energy for the system with a fixed number of protons and electrons [6,11,12,86,87].

2.2. Changing Protonation States of the OEC through the S-State Cycle

The mechanism of O_2 evolution involves both electron and proton transfer reactions [88–90]. Over the course of the reaction, cycle protons must be shed from the substrate waters. Coupled electron and proton transfers also keep the OEC catalyst from building up excess charge. The redox potential of a Mn with a protonated μ -oxo bridge or neutral terminal water ligand will be more positive than when the proton is lost [62–64]. The oxidation of Mn^{III} to Mn^{IV} lowers the pK_a of a terminal water ligand by as much as ten pH units [62–64]. Thus, the proton distribution will be strongly influenced by which Mn in the OEC is Mn^{III} or Mn^{IV} and conversely the oxidation state of the Mn will be influenced by the protonation state of the bridging oxygens and bound waters.

Experiments show one proton is lost between S_0 and S_1 and between S_2 and S_3 while 0 [91–94] to 0.3 [24] are lost on formation of S_2 . There is general agreement that in S_0 there is a proton on the oxygen bridging Mn1 and Mn4 (O5) that is lost forming S_1 . This leaves the terminal waters as having the only protons bound to the OEC beyond S_0 . There is also general agreement that W3 and W4 on the Ca^{II} will remain neutral in S_0 , S_1 , and S_2 [5].

The protonation states of W1 and W2 bound to Mn4 remain an open question. The Mn–O bond length in XFEL structures supports these waters being neutral in the well resolved S_1 (3443) structures where Mn4 is in the Mn^{III} oxidation state [21]. FTIR spectroscopy suggests formation of a Mn-bound hydroxyl in the multiline, 3444, S_2 state [95]. FTIR spectroscopy [96] and XFEL structures [97] support W1 and W2 being neutral in the 4443 S_2 isomer, while there being one hydroxyl and one water in the 3444 S_2 isomer [98].

DFT and QM/MM calculations must define the number of protons in the system and a number of different choices have been made. Calculations have used a hydroxyl on W2 of Mn4 in S_1 [99] and S_2 [32,100], fully protonated water in S_1 [101] and hydroxyl on W2 in S_2 [23] or fully protonated water in both S_1 and S_2 states [28]. Recent classical MCCE calculations, using a CE/MC method, found that at equilibrium there is a mixture of OECs with W2 being hydroxyl or water in the multi-line, 3444 S_2 state [102]. We are not referring to this situation as W2 being at its pK_a as the pH dependence does not follow the Henderson Hasselbalch equation. The finding that Mn4 bound H_2O and OH^- are close in energy may help explain the difficulty in defining the protonation state of W2 in this redox state. Thus, oxidation from S_1 to S_2 moves the proton affinity of W2 so that protonation hangs in the balance. There is little penalty to hold on to the proton, leading to little proton loss on forming S_2 . However, there is little energy needed to lose a proton, which is needed as the OEC moves into the S_3 state [21,31,41].

2.3. Changing Protonation States of Residues in the Protein through the Reaction Cycle

Changes in the protonation state of the OEC substrate water or the water produced in the BNC are required to complete the reaction. In addition, each reaction cycle induces changes in the protonation and conformation states of the rest of the protein [6,51,99,103]. Some of these changes are essential to the function as they lead to proton transfer away from the N-side and into the P-side of the protein in the membrane. CE/MC methods, which allow the whole protein to come to equilibrium with each protein redox state intermediate, have been used to evaluate the changes in protonation states through the S-state cycle in PSII [104] and through the reaction cycle in CcO [53,105]. It should be noted that introduction of a charge will shift the proton affinity of all nearby residues. However, to release a proton the pK_a start above the pH and shift to be below it; conversely proton binding requires the pK_a to shift from below to above the pH [3].

2.3.1. PSII Protonation State

The protonation of all residues in PSII were determined with the OEC in different S-states using the CE/MC program, MCCE [102]. The S-state structures optimized by QM/MM [11] were docked into the 3ARC structure [106]. Polar hydrogen positions were sampled. Explicit waters were included and subjected to GCMC sampling. Of the acidic and basic residues within 15 Å of the OEC, only D1-E329 and D1-H337 change protonation during the transition from S_0 to S_2 . There is a 50–80% probability that W2 will lose a proton going from the S_1 to S_2 state [102]. D1-E329, in the large channel described below, has a pK_a near the pH, so it increases its probability of having a proton bound as W2 is deprotonated. In addition, there is a small probability of proton transfer from W1 to D1-D61. The stability of the protonation states of groups near the OEC is highlighted when the pH is raised from 6 to 8 in the MCCE analysis [102]. Calculations show no protonation state change in any residue within 15 Å of the OEC except for D1-E329. At pH 6, D1-E329 acts as buffer during the S-state transition while it is fully deprotonated in all S-states at pH 8.

2.3.2. CcO Protonation State

In CcO protons need to be translocated across the membrane and thus residues must experience ionization state changes coupled to the BNC redox and protonation state cycle. There is a proton loading site (PLS) that transiently binds protons for release, which has been assumed to lie on the P-side of the protein relative to the BNC. The proton affinity of the PLS would increase when the protein is in the BNC states associated with proton loading and decrease to unload protons as the cycle progresses. A number of residues had been suggested to be the PLS including the propionate A [51,107] or propionate D [108] of heme a_3 , or H334, which is one of the ligands of Cu_B [109,110].

The stochastic MC analysis in MCCE was used to evaluate the identity of the PLS in an unbiased way [111]. Each of the four additions of an electron and a proton to the BNC through the P/F, O, E, R states is coupled to one proton pumped. Thus, the MCCE calculations broke the electron and proton transfers involving Heme a , E286 and the BNC that occur in each redox state transition into

six steps and the protonation states of all residues in the protein were determined. Observed changes in the probability of protonation of several heme propionic acids led to the identification of the PLS as a cluster of residues, instead of a single site. The detailed division of the reaction cycle shows the proton is loaded to the PLS when heme *a* is reduced, while the PLS releases its proton when a proton is transferred from E86 to the BNC. These results amplified previous models of CcO function [51].

3. Finding Water and Proton Transfer Pathways

Protons must be transferred through protein in a step-wise manner, with a proton donor passing it to a hydrogen bonded proton acceptor. Water, with a lone pair to accept a proton and a bound proton to donate, plays an important role in proton transfer via the Grotthuss mechanism. Thus, potential proton transfer pathways are identified as consisting of hydrogen bonded chains of water, with protonatable residues providing sites for metastable proton transfer intermediates. The rate of proton transfer will depend on the probability that a pathway is connected and on the free energy of injecting a proton into the path.

3.1. Methods to Find Water and Proton Pathways

There are several methods to find proton pathways. The simplest is to find connected cavities with programs such as Caver [112] or Hole [113]. Other programs such as Dowser++ carry out a semi-empirical analysis to evaluate the likelihood that waters will reside in these cavities [114]. These programs analyze a single protein structure and determine if there is sufficient room for water, with a defined radius (generally 1.4 Å). The simplicity of these methods makes them ideal for the first analysis of a crystal structure.

MD trajectories for protein embedded in explicit water will show many waters traveling within the protein. Grand Canonical Monte Carlo (GCMC) sampling also allows waters to come to equilibrium, moving between the protein and solvent, generally in a structure with a fixed protein backbone. Both MD and GCMC methods use classical force fields to determine the probability of water being at each position.

The waters in MD trajectories can be analyzed in numerous ways. For example, the distribution of the number of waters around a key residue through the trajectory or the probability that proton donor and acceptors sites will be connected via waters can be found [115]. Potential of mean force (PMF) methods allow us to determine the energy of waters or protons passing through a specified channel [116,117]. The calculations start from a MD trajectory and determine the energy of the particle at each location along the path. This can find the barrier for transfer as well as the low energy positions where a water or proton may be trapped. One disadvantage is that the pathway to be evaluated is constrained to path(s) found in the initial MD trajectory. Also, as this uses classical MD methods, the protonation states are fixed and cannot come to equilibrium with any changes as the particle moves along the path.

Markov state models (MSM) [118] have been applied to analyze which dynamic motions are coupled to water cavity opening. Here at each point in a trajectory the cavity hydration is correlated with a few other collective geometric variables [118]. The constructed MSM trajectories are projected into the collective variable space, and clustered into microstates, then into several macrostates, which vary from a dry and compact cavity macrostate to one that is wet and expanded. The MSM transition matrix can be used to compute the mean first passage times (MFPTs) of the opening (to wet and expanded) and closing (to dry and compact) cavity transitions [118].

Hydrogen bond connections made in many snapshots in an MD trajectory or the many accepted microstates of an GCMC analysis can be subjected to a network analysis [119]. Programs such as Cytoscape [120] and Gephi [121], permit visualization of the network (see Figures 3b and 4). MCCE [70] carries out GCMC analysis of the water orientation and occupancy and the protonation state and proton positions of residues in the whole protein. Network analysis [119] then generates a hydrogen bond matrix for the resultant Boltzmann distribution. Long-range connections between residues

Continuum electrostatics/Monte Carlo (CE/MC) studies [126] were carried out on the 2AXT structure [130] to calculate the p of D1-D61, D1-E65, D2-E312, D2-K317, PsbO-D158, PsbO-D222, PsbO-D224, PsbO-H228, and PsbO-E229 in the broad channel, using the Karlsberg program [71]. The pK_as were found to increase monotonically moving from the OEC to the lumen. This observation led to the proposal that the broad channel will conduct protons outward, with the gradient of the proton affinity slowing proton leakage back into the protein.

Recently, combined MD and continuum electrostatics studies on 3ARC [106] cyanobacterial PSII and 3JCU [133] of spinach PSII showed how the properties of the large channel in cyanobacterial PSII (running through subunits denoted PsbU/V) and spinach PSII (in PsbP/PsbQ) are conserved [134,135].

The broad channel also runs through the PsbO subunit in PSII. In the broad channel, pairs of acidic amino acids surrounded by water clusters have been proposed to facilitate the proton transfer to the lumen [136]. A truncated PsbO-β subunit was crystallized at pH 6 and pH 10. MD simulations were carried out on the two structures with D102, which is in a pair with E97 in the loop of PsbO barrel of PSII, in different protonation states [125]. These two acidic residues are conserved. D102 is fixed in its protonated form in the pH 6 MD simulation and deprotonated in the simulation run on the pH 10 structure. All other carboxylates are ionized in both MD simulations. When D102 is protonated D102-E97 associates with one and five waters in an orderly manner that can conduct protons via a Grotthuss-type mechanism. Thus, the cluster may trap a proton preventing its backflow to the OEC. The cluster is disrupted at pH 10 when both carboxylates are ionized.

D1-D61 and D2-K317 are both found at the entry to the broad channel, near a Cl found in the 3ARC PSII structure [106]. Experiments [137] show that Cl is required for the OEC to progress beyond the S₂ state. MD and MCCE simulations [138] show that Cl removal results in the formation of a salt bridge between D1-D61 and D2-K317 blocking proton transfer through the broad channel [139]. In addition, MCCE calculations suggest the loss of the Cl [138,139] will change the protonation states of residues near the OEC and increase the number of protons lost when the OEC is oxidized from S₁ to S₂ [102].

There are several physical methods that can help follow the pathway of water, O₂, and protons [123,128,129,132]. Radiolytic footprinting can trace the residues surrounding water channels and also buried waters [140,141]. Exposure of the protein to X-rays produces OH· which will oxidatively modify nearby amino acids. These are then identified by mass spectrometry. Modified residues are found along the broad and large channels [140,142].

Mutagenesis studies have also modified the residues around the OEC to understand their role in assisting proton exit during the S-state transitions. D1-D61, which is hydrogen bonded to the W1 ligand of Mn₄ is at the entry of the narrow and broad channels (Figure 3b). It can accept protons released from the OEC during water splitting and pass them into these channels. D1-D61N [143] lowers the O₂ evolution efficiency. FTIR spectroscopy on D1-D61A [144] shows changes in the hydrogen bond network around the OEC. MCCE studies [102] on D1-D61A mutants show more proton loss to the solvent on the S₁ to S₂ state transition relative to that found with the wild-type protein.

Another residue that is also part of the proton exit pathway is D2-K317. FTIR spectroscopy [145] on the mutants D2-K317A, K317R, K317Q, and K317E find the hydrogen bond network is perturbed. The FTIR measurements suggest conformational changes in the protein backbone that may help disrupt proton movement.

3.3. Water and Proton Transfer Pathways in CcO

CcO is a proton pump, translocating protons from N- to P-side of the membrane through water filled channels and cavities. It requires gates on both N- and P-side to prevent protons from traveling in the wrong direction. The interior of CcO on the N-side is relatively non-polar, so that the waters and polar residues in the two proton channels (D and K) are easy to see in the crystal structures. The functionality of residues in these channels has been supported by the impact of their mutation on the function [146]. The D-channel transports both chemical protons to the BNC and pumped protons to the PLS, while the K-channel carries only chemical protons [147–149] (see Figure 1b). While the

N-side channels are visible in crystal structures, no path from the D-channel to the PLS is found in the crystal structures. As will be described below MD simulations varying the protonation states of key residues are beginning to show the proposed connections.

3.3.1. The P-Side Exit Path

In contrast to the N-side, the P-side of CcO contains many buried polar residues that surround the PLS. Thus, it was not possible to identify the pathway to the P-side by inspection. Electrostatic calculations on bovine CcO, suggested that K171/D173 in subunit II to be promising candidates to lie on the proton exit pathway. These well-conserved residues had neutral and ionized forms close in energy as determined by CE/MC analysis so could bind and release protons with little change in energy [150]. Inspection of the Bovine CcO structure suggested an H-channel traveling from N-side to P-side [49,151,152], supported by mutagenesis [152]. However, mutations of the analogous H-channel residues in *Rb. sphaeroides* CcO [153] and yeast [154] did not support this assignment. Recent simulations with MCCE hydrogen bond network analysis in *Rb. sphaeroides* CcO [119] proposed a different proton exit pathway via N96, T100, S168 (*Rb. sphaeroides* numbering) with the exit close to H93/E182.

3.3.2. The Path through the Protein

In CcO, channels must be able to open and close to ensure that protons are bound from the N-side and released to the P-side. The hydration level of a cavity can serve as a switch, where the hydrated cavity promotes proton translocation and the dehydrated cavity blocks the proton path [51]. One of the key features of CcO is an orderly decision to transfer protons to the PLS for pumping or to the BNC for chemistry, both via the D-channel. Crystal structures, while containing many waters, often appear to be relatively dry. Thus, the CcO crystal structures do not show connections from the D-channel to the PLS, ~ 10 Å away, or to the BNC.

MD analysis found that protonating one of the heme propionic acids causes the rearrangement of a loop, which is anchored by a hydrogen bond to the ionized propionic acid. The loop opening creates a cavity (the Glu cavity) that fills with water in nanoseconds in a MD simulation [108,118]. This cavity stabilizes the charge on the isolated E286 (see Figure 1b), which is a likely proton transfer site [108]. E286 has a pK_a in the dry, resting protein over 10 [105]. The coupling of the conformational changes of key residues to cavity opening were characterized by MSM analysis, allowing key hydrogen bond connections to be identified [118].

MD snapshots of *Rb. sphaeroides* CcO were subjected to MCCE network analysis [119]. Well hydrated MD snapshots show connections from a polar residue cluster on the N-side of the protein through the D-channel to the PLS and on to the P-side of the protein (Figure 4). However, the K-channel remains disconnected [155]. The exit of the hydrogen bond network [119] is near several identified water exit pathways [118]. The network analysis was also carried out on snapshots from MD trajectories run changing the protonation states of key residues that lead to changes in hydration. The highly interconnected clusters (shown as circles in Figure 4) are always present, while the connections between clusters are made and broken by changes in hydration. The Glu cavity must be hydrated to form connections between the D-channel and both the BNC and PLS [119]. A small water cavity, which may be controlled by the hydrophobic pair of I99 and L255B, is proposed to be able to open and close the proton path between the PLS and the P-side preventing back flow [119].

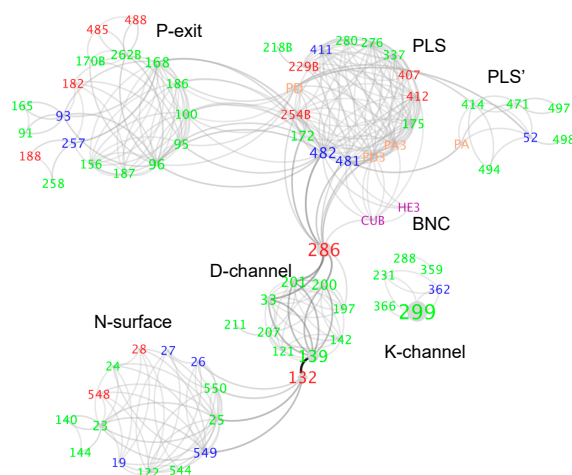


Figure 4. Hydrogen bond network in *Rb. sphaeroides* CcO [119]. The network is divided into circular clusters with well-connected residues shown as: N-surface, D-channel, K-channel, BNC, PLS, PLS', P-exit. Residues are shown as individual nodes, labeled by residue number, followed by B to identify residues in subunit II. Heme a_3 is labeled as HE3, while Cu_B as CUB, propionic acids of heme a_3 as PA3/PD3, propionic acids of heme a as PA/PD. The labels are colored based on amino acid type; red: acid; blue: base; green: neutral polar; orange: propionic acid; purple: BNC. The larger nodes and darker edges show more important connections in the network analysis.

There has been a discussion about the role of the Glu cavity hydration for controlling proton transfer from the D-channel to the PLS. One critical question is how such a well hydrated cavity can block leaks from the P-side back to the D-channel or the BNC [48]. In addition, while the propionate D of heme a_3 , triggers the hydration of the cavity, propionate A of heme a_3 may have a higher proton affinity. The question arises if this proton transfer to propionate A would rapidly close the cavity [156]. However, in the MD simulations while the cavity opens quickly, it closes more slowly so the shift of a proton within the PLS may lead to only slow dehydration [118].

The orientation of water chains within the channels has also been proposed to act as a switch to control proton transport, promoting unidirectional proton pumping. It has been suggested that the electric field between heme a and the BNC will orient water, favoring Grotthuss proton transfer in one direction, especially when there is a single line of waters in a relatively dry channel [157]. However, the electric field is unlikely to be strong enough to explain the directionality of the proton pump [48,86] and given the slow rate of water reorientation after transfer of one proton the overall transfer rate may not support efficient CcO turnover by this mechanism [48,158].

3.3.3. Testing the Location of Water Channel Experimentally

Hydrogen–deuterium exchange measurements have been used to monitor the residues that have greater access to the solvent during turnover in CcO [159]. Various regions of the protein backbone are identified that may run along proton channels. Regions in the proposed hydrogen bond network do show enhanced exchange in a functioning CcO [119]. One interesting observation is that under conditions when the K-pathway is assumed to be active the D-pathway shows reduced H/D exchange, suggesting a mechanism that can provide alternating access to the two channels.

4. Conclusions

The OEC of PSII catalyzes the difficult oxidation of water using only earth abundant elements so that water, the universal biological solvent, can be the terminal electron donor. CcO uses the energy released on reduction of O₂, the product of the OEC reaction, to add to the electrochemical proton gradient. The problems of current interest are somewhat different in the two proteins. In PSII the open questions focus on the details of the S-state cycle, asking how the OEC structure, electron distribution,

and protonation states prepare the system for the O–O bond formation. There are several well defined water channels which are assumed to be always open for their business of transporting water, O₂, and protons. In contrast, in CcO it is the identification of the proton pathways and the method by which they are controlled that poses the most challenging questions. A variety of computational approaches—including QM/MM, MD, and CE/MC have been applied to address these questions. Each method has its strengths and weaknesses, but in combination they are producing a picture of the detailed mechanisms of these two important proteins.

Author Contributions: D.K. and X.C. contributed to the origin and draft preparation focused on PSII and CcO respectively. U.K., Y.Z., J.M., and M.M. added to the review of methodology. M.R.G. Gunner reviewed and edited the manuscript.

Funding: This research was funded by the Department of Energy Basic Energy Sciences grant number DE-SC0001423 and the National Science Foundation grant MCB-1519640.

Conflicts of Interest: The authors declare no conflict of interest.

References

1. Falkowski, P.G.; Godfrey, L.V. Electrons, life and the evolution of Earth's oxygen cycle. *Philos. Trans. R. Soc. Lond. B Biol. Sci.* **2008**, *363*, 2705–2716. [[CrossRef](#)] [[PubMed](#)]
2. Gunner, M.R.; Amin, M.; Zhu, X.; Lu, J. Molecular mechanisms for generating transmembrane proton gradients. *Biochim. Biophys. Acta* **2013**, *1827*, 892–913. [[CrossRef](#)] [[PubMed](#)]
3. Gunner, M.R.; Koder, R. The design features cells use to build their transmembrane proton gradient. *Phys. Biol.* **2017**, *14*, 013001. [[CrossRef](#)] [[PubMed](#)]
4. Cox, N.; Messinger, J. Reflections on substrate water and dioxygen formation. *Biochim. Biophys. Acta* **2013**, *1827*, 1020–1030. [[CrossRef](#)] [[PubMed](#)]
5. Dau, H.; Zaharieva, I.; Haumann, M. Recent developments in research on water oxidation by photosystem II. *Curr. Opin. Chem. Biol.* **2012**, *16*, 3–10. [[CrossRef](#)] [[PubMed](#)]
6. Vinyard, D.J.; Brudvig, G.W. Progress toward a molecular mechanism of water oxidation in photosystem II. *Annu. Rev. Phys. Chem.* **2017**, *68*, 101–116. [[CrossRef](#)] [[PubMed](#)]
7. Styring, S.; Sjöholm, J.; Mamedov, F. Two tyrosines that changed the world: Interfacing the oxidizing power of photochemistry to water splitting in photosystem II. *Biochim. Biophys. Acta* **2012**, *1817*, 76–87. [[CrossRef](#)]
8. Joliot, P. Period-four oscillations of the flash-induced oxygen formation in photosynthesis. In *Discoveries in Photosynthesis*; Govindjee, B.J.T., Gest, H., Allen, J.F., Eds.; Springer: Berlin/Heidelberg, Germany, 2005; Volume 20, pp. 371–378, ISBN 978-1-4020-3323-0.
9. Kok, B.; Forbush, B.; McGloin, M. Cooperation of charges in photosynthetic O₂ evolution-I. A linear four step mechanism. *Photochem. Photobiol.* **1970**, *11*, 457–475. [[CrossRef](#)]
10. Nilsson, H.; Cournac, L.; Rappaport, F.; Messinger, J.; Lavergne, J. Estimation of the driving force for dioxygen formation in photosynthesis. *Biochim. Biophys. Acta* **2016**, *1857*, 23–33. [[CrossRef](#)]
11. Askerka, M.; Brudvig, G.W.; Batista, V.S. The O₂-evolving complex of photosystem II: Recent insights from quantum mechanics/molecular mechanics (QM/MM), extended X-ray absorption fine structure (EXAFS), and femtosecond X-ray crystallography data. *Acc. Chem. Res.* **2017**, *50*, 41–48. [[CrossRef](#)]
12. Siegbahn, P.E.M. Water oxidation mechanism in photosystem II, including oxidations, proton release pathways, O–O bond formation and O₂ release. *Biochim. Biophys. Acta* **2013**, *1827*, 1003–1019. [[CrossRef](#)] [[PubMed](#)]
13. Yano, J.; Kern, J.; Sauer, K.; Latimer, M.J.; Pushkar, Y.; Biesiadka, J.; Loll, B.; Saenger, W.; Messinger, J.; Zouni, A.; et al. Where water is oxidized to dioxygen: Structure of the photosynthetic Mn₄Ca cluster. *Science* **2006**, *314*, 821–825. [[CrossRef](#)] [[PubMed](#)]
14. Young, I.D.; Ibrahim, M.; Chatterjee, R.; Gul, S.; Fuller, F.; Koroidov, S.; Brewster, A.S.; Tran, R.; Alonso-Mori, R.; Kroll, T.; et al. Structure of photosystem II and substrate binding at room temperature. *Nature* **2016**, *540*, 453–457. [[CrossRef](#)] [[PubMed](#)]
15. Ferreira, K.N.; Iverson, T.M.; Maghlaoui, K.; Barber, J.; Iwata, S. Architecture of the photosynthetic oxygen-evolving center. *Science* **2004**, *303*, 1831–1838. [[CrossRef](#)]

16. Galstyan, A.; Robertazzi, A.; Knapp, E.W. Oxygen-Evolving Mn Cluster in Photosystem II: The Protonation Pattern and Oxidation State in the High-Resolution Crystal Structure. *J. Am. Chem. Soc.* **2012**, *134*, 7442–7449. [[CrossRef](#)] [[PubMed](#)]
17. Yano, J.; Kern, J.; Irrgang, K.-D.; Latimer, M.J.; Bergmann, U.; Glatzel, P.; Pushkar, Y.; Biesiadka, J.; Loll, B.; Sauer, K.; et al. X-ray damage to the Mn₄Ca complex in single crystals of photosystem II: A case study for metalloprotein crystallography. *Proc. Natl. Acad. Sci. USA* **2005**, *102*, 12047–12052. [[CrossRef](#)] [[PubMed](#)]
18. Kern, J.; Tran, R.; Alonso-Mori, R.; Koroidov, S.; Echols, N.; Hattne, J.; Ibrahim, M.; Gul, S.; Laksmono, H.; Sierra, R.G.; et al. Taking snapshots of photosynthetic water oxidation using femtosecond X-ray diffraction and spectroscopy. *Nat. Commun.* **2014**, *5*, 4371. [[CrossRef](#)] [[PubMed](#)]
19. Kern, J.; Alonso-Mori, R.; Tran, R.; Hattne, J.; Gildea, R.J.; Echols, N.; Glöckner, C.; Hellmich, J.; Laksmono, H.; Sierra, R.G.; et al. Simultaneous femtosecond X-ray spectroscopy and diffraction of photosystem II at room temperature. *Science* **2013**, *340*, 491–495. [[CrossRef](#)]
20. Suga, M.; Akita, F.; Sugahara, M.; Kubo, M.; Nakajima, Y.; Nakane, T.; Yamashita, K.; Umena, Y.; Nakabayashi, M.; Yamane, T.; et al. Light-induced structural changes and the site of O=O bond formation in PSII caught by XFEL. *Nature* **2017**, *543*, 131–135. [[CrossRef](#)]
21. Suga, M.; Akita, F.; Hirata, K.; Ueno, G.; Murakami, H.; Nakajima, Y.; Shimizu, T.; Yamashita, K.; Yamamoto, M.; Ago, H.; et al. Native structure of photosystem II at 1.95 Å resolution viewed by femtosecond X-ray pulses. *Nature* **2015**, *517*, 99–103. [[CrossRef](#)]
22. Askerka, M.; Vinyard, D.J.; Wang, J.; Brudvig, G.W.; Batista, V.S. Analysis of the radiation-damage-free X-ray structure of photosystem II in light of EXAFS and QM/MM data. *Biochemistry* **2015**, *54*, 1713–1716. [[CrossRef](#)] [[PubMed](#)]
23. Ames, W.; Pantazis, D.A.; Krewald, V.; Cox, N.; Messinger, J.; Lubitz, W.; Neese, F. Theoretical evaluation of structural models of the S₂ state in the oxygen evolving complex of photosystem II: Protonation states and magnetic interactions. *J. Am. Chem. Soc.* **2011**, *133*, 19743–19757. [[CrossRef](#)] [[PubMed](#)]
24. Suzuki, H.; Sugiura, M.; Noguchi, T. Monitoring proton release during photosynthetic water oxidation in photosystem II by means of isotope-edited infrared spectroscopy. *J. Am. Chem. Soc.* **2009**, *131*, 7849–7857. [[CrossRef](#)] [[PubMed](#)]
25. Siegbahn, P.E.M. O–O bond formation in the S₄ state of the oxygen-evolving complex in photosystem II. *Chem. Eur. J.* **2006**, *12*, 9217–9227. [[CrossRef](#)] [[PubMed](#)]
26. Pal, R.; Negre, C.F.; Vogt, L.; Pokhrel, R.; Ertem, M.Z.; Brudvig, G.W.; Batista, V.S. S₀-State model of the oxygen-evolving complex of photosystem II. *Biochemistry* **2013**, *52*, 7703–7706. [[CrossRef](#)] [[PubMed](#)]
27. Lubner, S.; Rivalta, I.; Umena, Y.; Kawakami, K.; Shen, J.-R.; Kamiya, N.; Brudvig, G.W.; Batista, V.S. S₁-state model of the O₂-evolving complex of photosystem II. *Biochemistry* **2011**, *50*, 6308–6311. [[CrossRef](#)] [[PubMed](#)]
28. Askerka, M.; Wang, J.; Brudvig, G.W.; Batista, V.S. Structural changes in the oxygen-evolving complex of photosystem II induced by the S₁ to S₂ transition: A combined XRD and QM/MM study. *Biochemistry* **2014**, *53*, 6860–6862. [[CrossRef](#)]
29. Pantazis, D.A.; Ames, W.; Cox, N.; Lubitz, W.; Neese, F. Two interconvertible structures that explain the spectroscopic properties of the oxygen-evolving complex of photosystem II in the S₂ state. *Angew. Chem.* **2012**, *51*, 9935–9940. [[CrossRef](#)]
30. Askerka, M.; Wang, J.; Vinyard, D.J.; Brudvig, G.W.; Batista, V.S. S₃ state of the O₂-evolving complex of photosystem II: Insights from QM/MM, EXAFS, and Femtosecond X-ray Diffraction. *Biochemistry* **2016**, *55*, 981–984. [[CrossRef](#)]
31. Retegan, M.; Krewald, V.; Mamedov, F.; Neese, F.; Lubitz, W.; Cox, N.; Pantazis, D.A. A five-coordinate Mn(IV) intermediate in biological water oxidation: Spectroscopic signature and a pivot mechanism for water binding. *Chem. Sci.* **2015**, *7*, 72–84. [[CrossRef](#)]
32. Siegbahn, P.E.M. Substrate water exchange for the oxygen evolving complex in PSII in the S₁, S₂, and S₃ states. *J. Am. Chem. Soc.* **2013**, *135*, 9442–9449. [[CrossRef](#)]
33. Cox, N.; Pantazis, D.A.; Neese, F.; Lubitz, W. Biological water oxidation. *Acc. Chem. Res.* **2013**, *46*, 1588–1596. [[CrossRef](#)]
34. Bovi, D.; Narzi, D.; Guidoni, L. The S₂ state of the oxygen-evolving complex of photosystem II explored by QM/MM dynamics: Spin surfaces and metastable states suggest a reaction path towards the S₃ state. *Angew. Chem.* **2013**, *52*, 11744–11749. [[CrossRef](#)]

35. Pantazis, D.A.; Orio, M.; Petrenko, T.; Zein, S.; Lubitz, W.; Messinger, J.; Neese, F. Structure of the oxygen-evolving complex of photosystem II: Information on the S₂ state through quantum chemical calculation of its magnetic properties. *Phys. Chem. Chem. Phys.* **2009**, *11*, 6788–6798. [[CrossRef](#)]
36. Paul, S.; Cox, N.; Pantazis, D.A. What Can We Learn from a Biomimetic Model of Nature's Oxygen-Evolving Complex? *Inorg. Chem.* **2017**, *56*, 3875–3888. [[CrossRef](#)] [[PubMed](#)]
37. Boussac, A.; Rutherford, A.W. Comparative study of the g=4.1 EPR signals in the S₂ state of photosystem II. *Biochim. Biophys. Acta* **2000**, *1457*, 145–156. [[CrossRef](#)]
38. Cox, N.; Retegan, M.; Neese, F.; Pantazis, D.A.; Boussac, A.; Lubitz, W. Electronic structure of the oxygen-evolving complex in photosystem II prior to O–O bond formation. *Science* **2014**, *345*, 804–808. [[CrossRef](#)]
39. Siegbahn, P.E.M. Mechanisms for proton release during water oxidation in the S₂ to S₃ and S₃ to S₄ transitions in photosystem II. *Phys. Chem. Chem. Phys.* **2012**, *14*, 4849–4856. [[CrossRef](#)]
40. Narzi, D.; Mattioli, G.; Bovi, D.; Guidoni, L. A spotlight on the compatibility between XFEL and ab Initio structures of the oxygen evolving complex in photosystem II. *Chem. Eur. J.* **2017**, *23*, 6969–6973. [[CrossRef](#)]
41. Wang, J.; Askerka, M.; Brudvig, G.W.; Batista, V.S. Crystallographic Data Support the Carousel Mechanism of Water Supply to the Oxygen-Evolving Complex of Photosystem II. *ACS Energy Lett.* **2017**, *2*, 2299–2306. [[CrossRef](#)]
42. Guo, Y.; Li, H.; He, L.-L.; Zhao, D.-X.; Gong, L.-D.; Yang, Z.-Z. The open-cubane oxo-oxyl coupling mechanism dominates photosynthetic oxygen evolution: A comprehensive DFT investigation on O–O bond formation in the S₄ state. *Phys. Chem. Chem. Phys.* **2017**, *19*, 13909–13923. [[PubMed](#)]
43. Siegbahn, P.E.M. Nucleophilic water attack is not a possible mechanism for O–O bond formation in photosystem II. *Proc. Natl. Acad. Sci. USA* **2017**, *114*, 4966–4968. [[CrossRef](#)] [[PubMed](#)]
44. Kern, J.; Chatterjee, R.; Young, I.D.; Fuller, F.D.; Lassalle, L.; Ibrahim, M.; Gul, S.; Fransson, T.; Brewster, A.S.; Alonso-Mori, R.; et al. Structures of the intermediates of Kok's photosynthetic water oxidation clock. *Nature* **2018**, *563*, 421–425. [[CrossRef](#)]
45. Ugur, I.; Rutherford, A.W.; Kaila, V.R.I. Redox-coupled substrate water reorganization in the active site of Photosystem II—The role of calcium in substrate water delivery. *Biochim. Biophys. Acta* **2016**, *1857*, 740–748. [[CrossRef](#)] [[PubMed](#)]
46. Popović, D.M. Current advances in research of cytochrome c oxidase. *Amino Acids* **2013**, *45*, 1073–1087. [[CrossRef](#)] [[PubMed](#)]
47. Rich, P.R. Mitochondrial cytochrome c oxidase: Catalysis, coupling and controversies. *Biochem. Soc. Trans.* **2017**, *45*, 813–829. [[CrossRef](#)] [[PubMed](#)]
48. Wikström, M.; Sharma, V. Proton pumping by cytochrome c oxidase—A 40 year anniversary. *Biochim. Biophys. Acta Bioenerg.* **2018**, *1859*, 692–698. [[CrossRef](#)] [[PubMed](#)]
49. Yoshikawa, S.; Shimada, A. Reaction mechanism of cytochrome c oxidase. *Chem. Rev.* **2015**, *115*, 1936–1989. [[CrossRef](#)]
50. Sousa, F.L.; Alves, R.J.; Ribeiro, M.A.; Pereira-Leal, J.B.; Teixeira, M.; Pereira, M.M. The superfamily of heme–copper oxygen reductases: Types and evolutionary considerations. *Biochim. Biophys. Acta* **2012**, *1817*, 629–637. [[CrossRef](#)]
51. Kaila, V.R.I.; Verkhovskiy, M.I.; Wikström, M. Proton-coupled electron transfer in cytochrome oxidase. *Chem. Rev.* **2010**, *110*, 7062–7081. [[CrossRef](#)]
52. Brändén, G.; Gennis, R.B.; Brzezinski, P. Transmembrane proton translocation by cytochrome c oxidase. *Biochim. Biophys. Acta* **2006**, *1757*, 1052–1063. [[CrossRef](#)] [[PubMed](#)]
53. Faxén, K.; Gilderson, G.; Adelroth, P.; Brzezinski, P. A mechanistic principle for proton pumping by cytochrome c oxidase. *Nature* **2005**, *437*, 286–289. [[CrossRef](#)] [[PubMed](#)]
54. Proshlyakov, D.A.; Pressler, M.A.; DeMaso, C.; Leykam, J.F.; DeWitt, D.L.; Babcock, G.T. Oxygen activation and reduction in respiration: Involvement of redox-active tyrosine 244. *Science* **2000**, *290*, 1588–1591. [[CrossRef](#)]
55. Gorbikova, E.A.; Belevich, I.; Wikström, M.; Verkhovskiy, M.I. The proton donor for O–O bond scission by cytochrome c oxidase. *Proc. Natl. Acad. Sci. USA* **2008**, *105*, 10733–10737. [[CrossRef](#)] [[PubMed](#)]
56. Adelroth, P.; Ek, M.; Brzezinski, P. Factors determining electron-transfer rates in cytochrome c oxidase: Investigation of the oxygen reaction in the *R. sphaeroides* enzyme. *Biochim. Biophys. Acta* **1998**, *1367*, 107–117. [[CrossRef](#)]

57. Verkhovskiy, M.I.; Morgan, J.E.; Wikström, M. Oxygen binding and activation: Early steps in the reaction of oxygen with cytochrome c oxidase. *Biochemistry* **1994**, *33*, 3079–3086. [[CrossRef](#)] [[PubMed](#)]
58. Belevich, I.; Bloch, D.A.; Belevich, N.; Wikström, M.; Verkhovskiy, M.I. Exploring the proton pump mechanism of cytochrome c oxidase in real time. *Proc. Natl. Acad. Sci. USA* **2007**, *104*, 2685–2690. [[CrossRef](#)] [[PubMed](#)]
59. Blomberg, M.R.A. Mechanism of Oxygen Reduction in Cytochrome c Oxidase and the Role of the Active Site Tyrosine. *Biochemistry* **2016**, *55*, 489–500. [[CrossRef](#)] [[PubMed](#)]
60. Han Du, W.-G.; Götz, A.W.; Noodleman, L. A water dimer shift activates a proton pumping pathway in the P_r→F Transition of *ba*₃ cytochrome c oxidase. *Inorg. Chem.* **2018**, *57*, 1048–1059. [[CrossRef](#)] [[PubMed](#)]
61. Gunner, M.R.; Madeo, J.; Zhu, Z. Modification of quinone electrochemistry by the proteins in the biological electron transfer chains: Examples from photosynthetic reaction centers. *J. Bioenerg. Biomembr.* **2008**, *40*, 509–519. [[CrossRef](#)]
62. Limburg, J.; Vrettos, J.S.; Liable-Sands, L.M.; Rheingold, A.L.; Crabtree, R.H.; Brudvig, G.W. A functional model for O–O bond formation by the O₂-evolving complex in photosystem II. *Science* **1999**, *283*, 1524–1527. [[CrossRef](#)] [[PubMed](#)]
63. Chen, H.; Tagore, R.; Das, S.; Incarvito, C.; Faller, J.W.; Crabtree, R.H.; Brudvig, G.W. General synthesis of di- μ -oxo dimanganese complexes as functional models for the oxygen evolving complex of photosystem II. *Inorg. Chem.* **2005**, *44*, 7661–7670. [[CrossRef](#)]
64. Amin, M.; Vogt, L.; Vassiliev, S.; Rivalta, I.; Sultan, M.M.; Bruce, D.; Brudvig, G.W.; Batista, V.S.; Gunner, M.R. Electrostatic effects on proton coupled electron transfer in oxomanganese complexes inspired by the oxygen-evolving complex of photosystem II. *J. Phys. Chem. B* **2013**, *117*, 6217–6226. [[CrossRef](#)] [[PubMed](#)]
65. Song, Y.; Mao, J.; Gunner, M.R. Electrostatic environment of hemes in proteins: pK_as of hydroxyl ligands. *Biochemistry* **2006**, *45*, 7949–7958. [[CrossRef](#)] [[PubMed](#)]
66. Gunner, M.R.; Baker, N.A. Continuum electrostatics approaches to calculating pK_as and E_ms in proteins. *Meth. Enzymol.* **2016**, *578*, 1–20. [[PubMed](#)]
67. Nielsen, J.E.; Gunner, M.R.; García-Moreno, B.E. The pK_a Cooperative: A collaborative effort to advance structure-based calculations of pK_a values and electrostatic effects in proteins. *Proteins* **2011**, *79*, 3249–3259. [[CrossRef](#)] [[PubMed](#)]
68. Alexov, E.; Mehler, E.L.; Baker, N.; Baptista, A.M.; Huang, Y.; Milletti, F.; Nielsen, J.E.; Farrell, D.; Carstensen, T.; Olsson, M.H.M.; et al. Progress in the prediction of pK_a values in proteins. *Proteins* **2011**, *79*, 3260–3275. [[CrossRef](#)]
69. Kieseritzky, G.; Knapp, E.-W. Optimizing pK_a computation in proteins with pH adapted conformations. *Proteins* **2008**, *71*, 1335–1348. [[CrossRef](#)] [[PubMed](#)]
70. Song, Y.; Mao, J.; Gunner, M.R. MCCE2: Improving protein pK_a calculations with extensive side chain rotamer sampling. *J. Comput. Chem.* **2009**, *30*, 2231–2247. [[CrossRef](#)] [[PubMed](#)]
71. Rabenstein, B. *Karlsberg Online Manual*; Freie Universität: Berlin, Germany, 1999.
72. Gunner, M.R.; Alexov, E. A pragmatic approach to structure based calculation of coupled proton and electron transfer in proteins. *Biochim. Biophys. Acta* **2000**, *1458*, 63–87. [[CrossRef](#)]
73. Di Russo, N.V.; Estrin, D.A.; Martí, M.A.; Roitberg, A.E. pH-Dependent conformational changes in proteins and their effect on experimental pK_as: The case of Nitrophorin 4. *PLoS Comput. Biol.* **2012**, *8*, e1002761. [[CrossRef](#)] [[PubMed](#)]
74. Zheng, Y.; Cui, Q. Microscopic mechanisms that govern the titration response and pK_a values of buried residues in *Staphylococcal nuclease* mutants. *Proteins* **2017**, *85*, 268–281. [[PubMed](#)]
75. Cruzeiro, V.W.D.; Amaral, M.S.; Roitberg, A.E. Redox potential replica exchange molecular dynamics at constant pH in AMBER: Implementation and validation. *J. Chem. Phys.* **2018**, *149*, 072338. [[CrossRef](#)] [[PubMed](#)]
76. Damjanovic, A.; Miller, B.T.; Okur, A.; Brooks, B.R. Reservoir pH replica exchange. *J. Chem. Phys.* **2018**, *149*, 072321. [[CrossRef](#)] [[PubMed](#)]
77. Lee, J.; Miller, B.T.; Brooks, B.R. Computational scheme for pH-dependent binding free energy calculation with explicit solvent. *Protein Sci.* **2016**, *25*, 231–243. [[CrossRef](#)] [[PubMed](#)]
78. Machuqueiro, M.; Baptista, A.M. Is the prediction of pK_a values by constant-pH molecular dynamics being hindered by inherited problems? *Proteins* **2011**, *79*, 3437–3447. [[CrossRef](#)] [[PubMed](#)]
79. Machuqueiro, M.; Baptista, A.M. Molecular dynamics at constant pH and reduction potential: Application to cytochrome c(3). *J. Am. Chem. Soc.* **2009**, *131*, 12586–12594. [[CrossRef](#)]

80. Radak, B.K.; Chipot, C.; Suh, D.; Jo, S.; Jiang, W.; Phillips, J.C.; Schulten, K.; Roux, B. Correction to constant-pH molecular dynamics simulations for large biomolecular systems. *J. Chem. Theory Comput.* **2018**, *14*, 6748–6749. [[CrossRef](#)]
81. Leontyev, I.V.; Stuchebrukhov, A.A. Polarizable molecular interactions in condensed phase and their equivalent nonpolarizable models. *J. Chem. Phys.* **2014**, *141*, 014103. [[CrossRef](#)]
82. Blomberg, M.R.A.; Borowski, T.; Himo, F.; Liao, R.-Z.; Siegbahn, P.E.M. Quantum chemical studies of mechanisms for metalloenzymes. *Chem. Rev.* **2014**, *114*, 3601–3658. [[CrossRef](#)]
83. Hohenberg, P.; Kohn, W. Inhomogeneous electron gas. *Phys. Rev.* **1964**, *136*, B864–B871. [[CrossRef](#)]
84. Thiel, W. Semiempirical quantum-chemical methods: Semiempirical quantum-chemical methods. *Wiley Interdiscip. Rev. Comput. Mol. Sci.* **2014**, *4*, 145–157. [[CrossRef](#)]
85. Warshel, A.; Levitt, M. Theoretical studies of enzymic reactions: Dielectric, electrostatic and steric stabilization of the carbonium ion in the reaction of lysozyme. *J. Mol. Biol.* **1976**, *103*, 227–249. [[CrossRef](#)]
86. Blomberg, M.R.A.; Siegbahn, P.E.M. The mechanism for proton pumping in cytochrome c oxidase from an electrostatic and quantum chemical perspective. *Biochim. Biophys. Acta* **2012**, *1817*, 495–505. [[CrossRef](#)] [[PubMed](#)]
87. Blomberg, M.R.A.; Siegbahn, P.E.M. Quantum chemistry applied to the mechanisms of transition metal containing enzymes—Cytochrome c oxidase, a particularly challenging case. *J. Comput. Chem.* **2006**, *27*, 1373–1384. [[CrossRef](#)] [[PubMed](#)]
88. Dau, H.; Haumann, M. The manganese complex of photosystem II in its reaction cycle—Basic framework and possible realization at the atomic level. *Coord. Chem. Rev.* **2008**, *252*, 273–295. [[CrossRef](#)]
89. Debus, R.J. The manganese and calcium ions of photosynthetic oxygen evolution. *Biochim. Biophys. Acta* **1992**, *1102*, 269–352. [[CrossRef](#)]
90. Brudvig, G.W. Water oxidation chemistry of photosystem II. *Philos. Trans. R. Soc. Lond. B Biol. Sci.* **2008**, *363*, 1211–1219. [[CrossRef](#)]
91. Brettel, K.; Schlodder, E.; Witt, H.T. Nanosecond reduction kinetics of photooxidized chlorophyll-aII (P-680) in single flashes as a probe for the electron pathway, H⁺-release and charge accumulation in the O₂-evolving complex. *Biochim. Biophys. Acta* **1984**, *766*, 403–415. [[CrossRef](#)]
92. Rappaport, F.; Lavergne, J. Proton release during successive oxidation steps of the photosynthetic water oxidation process: Stoichiometries and pH dependence. *Biochemistry* **1991**, *30*, 10004–10012. [[CrossRef](#)]
93. Jahns, P.; Junge, W. Proton release during the four steps of photosynthetic water oxidation: Induction of 1:1:1:1 pattern due to lack of chlorophyll a/b binding proteins. *Biochemistry* **1992**, *31*, 7398–7403. [[CrossRef](#)]
94. Lavergne, J.; Junge, W. Proton release during the redox cycle of the water oxidase. *Photosynth. Res.* **1993**, *38*, 279–296. [[CrossRef](#)] [[PubMed](#)]
95. Noguchi, T. FTIR detection of water reactions in the oxygen-evolving centre of photosystem II. *Philos. Trans. R. Soc. Lond. B Biol. Sci.* **2008**, *363*, 1189–1195. [[CrossRef](#)] [[PubMed](#)]
96. Pokhrel, R.; Brudvig, G.W. Oxygen-evolving complex of photosystem II: Correlating structure with spectroscopy. *Phys. Chem. Chem. Phys.* **2014**, *16*, 11812–11821. [[CrossRef](#)] [[PubMed](#)]
97. Koua, F.H.M.; Umena, Y.; Kawakami, K.; Shen, J.-R. Structure of Sr-substituted photosystem II at 2.1 Å resolution and its implications in the mechanism of water oxidation. *Proc. Natl. Acad. Sci. USA* **2013**, *110*, 3889–3894. [[CrossRef](#)] [[PubMed](#)]
98. Noguchi, T.; Sugiura, M. Structure of an active water molecule in the water-oxidizing complex of photosystem II as studied by FTIR spectroscopy. *Biochemistry* **2000**, *39*, 10943–10949. [[CrossRef](#)] [[PubMed](#)]
99. Siegbahn, P.E. Recent theoretical studies of water oxidation in photosystem II. *J. Photochem. Photobiol. B* **2011**, *104*, 94–99. [[CrossRef](#)]
100. Davis, K.M.; Pushkar, Y.N. Structure of the oxygen evolving complex of photosystem II at room temperature. *J. Phys. Chem. B* **2015**, *119*, 3492–3498. [[CrossRef](#)]
101. Robertazzi, A.; Galstyan, A.; Knapp, E.W. PSII manganese cluster: Protonation of W2, O5, O4 and His337 in the S₁ state explored by combined quantum chemical and electrostatic energy computations. *Biochim. Biophys. Acta* **2014**, *1837*, 1316–1321. [[CrossRef](#)]
102. Kaur, D.; Szejgis, W.; Mao, J.; Amin, M.; Reiss, K.M.; Askerka, M.; Cai, X.; Khaniya, U.; Zhang, Y.; Brudvig, G.W.; et al. Relative Stability of the S₂ isomers of the oxygen evolving complex of photosystem II. **2018**. revision.

103. Lee, H.J.; Reimann, J.; Huang, Y.; Adeloeth, P. Functional proton transfer pathways in the heme–copper oxidase superfamily. *Biochim. Biophys. Acta* **2012**, *1817*, 537–544. [[CrossRef](#)] [[PubMed](#)]
104. Amin, M.; Vogt, L.; Szejgis, W.; Vassiliev, S.; Brudvig, G.W.; Bruce, D.; Gunner, M.R. Proton-Coupled Electron Transfer During the S-State Transitions of the Oxygen-Evolving Complex of Photosystem II. *J Phys. Chem. B* **2015**, *119*, 7366–7377. [[CrossRef](#)] [[PubMed](#)]
105. Namslauer, A.; Aagaard, A.; Katsonouri, A.; Brzezinski, P. Intramolecular proton-transfer reactions in a membrane-bound proton pump: The effect of pH on the peroxy to ferryl transition in cytochrome c oxidase. *Biochemistry* **2003**, *42*, 1488–1498. [[CrossRef](#)] [[PubMed](#)]
106. Umena, Y.; Kawakami, K.; Shen, J.-R.; Kamiya, N. Crystal structure of oxygen-evolving photosystem II at a resolution of 1.9 Å. *Nature* **2011**, *473*, 55–60. [[CrossRef](#)] [[PubMed](#)]
107. Belevich, I.; Verkhovskiy, M.I.; Wikström, M. Proton-coupled electron transfer drives the proton pump of cytochrome c oxidase. *Nature* **2006**, *440*, 829–832. [[CrossRef](#)] [[PubMed](#)]
108. Goyal, P.; Lu, J.; Yang, S.; Gunner, M.R.; Cui, Q. Changing hydration level in an internal cavity modulates the proton affinity of a key glutamate in cytochrome c oxidase. *Proc. Natl. Acad. Sci. USA* **2013**, *110*, 18886–18891. [[CrossRef](#)] [[PubMed](#)]
109. Quenneville, J.; Popović, D.M.; Stuchebrukhov, A.A. Combined DFT and electrostatics study of the proton pumping mechanism in cytochrome c oxidase. *Biochim. Biophys. Acta* **2006**, *1757*, 1035–1046. [[CrossRef](#)]
110. Sugitani, R.; Medvedev, E.S.; Stuchebrukhov, A.A. Theoretical and computational analysis of the membrane potential generated by cytochrome c oxidase upon single electron injection into the enzyme. *Biochim. Biophys. Acta* **2008**, *1777*, 1129–1139. [[CrossRef](#)]
111. Lu, J.; Gunner, M.R. Characterizing the proton loading site in cytochrome c oxidase. *Proc. Natl. Acad. Sci. USA* **2014**, *111*, 12414–12419. [[CrossRef](#)]
112. Petřek, M.; Otyepka, M.; Banáš, P.; Košinová, P.; Koča, J.; Damborský, J. CAVER: A new tool to explore routes from protein clefts, pockets and cavities. *BMC Bioinform.* **2006**, *7*, 316. [[CrossRef](#)]
113. Smart, O.S.; Neduvilil, J.G.; Wang, X.; Wallace, B.A.; Sansom, M.S.P. HOLE: A program for the analysis of the pore dimensions of ion channel structural models. *J. Mol. Graph.* **1996**, *14*, 354–360. [[CrossRef](#)]
114. Morozenko, A.; Stuchebrukhov, A.A. Dowser++, a new method of hydrating protein structures. *Proteins* **2016**, *84*, 1347–1357. [[PubMed](#)]
115. Ge, X.; Gunner, M.R. Unraveling the mechanism of proton translocation in the extracellular half-channel of bacteriorhodopsin. *Proteins* **2016**, *84*, 639–654. [[PubMed](#)]
116. Kästner, J. Umbrella sampling. *Wiley Interdiscip. Rev. Comput. Mol. Sci.* **2011**, *1*, 932–942. [[CrossRef](#)]
117. Xu, J.; Voth, G.A. Free energy profiles for H⁺ conduction in the D-pathway of Cytochrome c Oxidase: A study of the wild type and N98D mutant enzymes. *Biochim. Biophys. Acta* **2006**, *1757*, 852–859. [[CrossRef](#)] [[PubMed](#)]
118. Son, C.Y.; Yethiraj, A.; Cui, Q. Cavity hydration dynamics in cytochrome c oxidase and functional implications. *Proc. Natl. Acad. Sci. USA* **2017**, *114*, E8830–E8836. [[CrossRef](#)] [[PubMed](#)]
119. Cai, X.; Haider, K.; Lu, J.; Radic, S.; Son, C.Y.; Cui, Q.; Gunner, M.R. Network analysis of a proposed exit pathway for protons to the P-side of cytochrome c oxidase. *Biochim. Biophys. Acta* **2018**, *1859*, 997–1005. [[CrossRef](#)] [[PubMed](#)]
120. Shannon, P.; Markiel, A.; Ozier, O.; Baliga, N.S.; Wang, J.T.; Ramage, D.; Amin, N.; Schwikowski, B.; Ideker, T. Cytoscape: A software environment for integrated models of biomolecular interaction networks. *Genome Res.* **2003**, *13*, 2498–2504. [[CrossRef](#)]
121. Bastian, M.; Heymann, S.; Jacomy, M. Gephi: An Open Source Software for Exploring and Manipulating Networks. In the Third International AAAI Conference on Weblogs and Social Media. 2009. Available online: <https://www.aaai.org/ocs/index.php/ICWSM/09/paper/view/154> (accessed on 10 December 2018).
122. Vogt, L.; Vinyard, D.J.; Khan, S.; Brudvig, G.W. Oxygen-evolving complex of Photosystem II: An analysis of second-shell residues and hydrogen-bonding networks. *Curr. Opin. Chem. Biol.* **2015**, *25*, 152–158. [[CrossRef](#)]
123. Ho, F.M.; Styring, S. Access channels and methanol binding site to the CaMn₄ cluster in photosystem II based on solvent accessibility simulations, with implications for substrate water access. *Biochim. Biophys. Acta* **2008**, *1777*, 140–153. [[CrossRef](#)]
124. Takaoka, T.; Sakashita, N.; Saito, K.; Ishikita, H. pK_a of a Proton-Conducting Water Chain in Photosystem II. *J. Phys. Chem. Lett.* **2016**, *7*, 1925–1932. [[CrossRef](#)] [[PubMed](#)]
125. Bondar, A.-N.; Dau, H. Extended protein/water H-bond networks in photosynthetic water oxidation. *Biochim. Biophys. Acta* **2012**, *1817*, 1177–1190. [[CrossRef](#)]

126. Ishikita, H.; Saenger, W.; Loll, B.; Biesiadka, J.; Knapp, E.-W. Energetics of a possible proton exit pathway for water oxidation in photosystem II. *Biochemistry* **2006**, *45*, 2063–2071. [[CrossRef](#)] [[PubMed](#)]
127. Saito, K.; Rutherford, A.W.; Ishikita, H. Energetics of proton release on the first oxidation step in the water-oxidizing enzyme. *Nat. Commun.* **2015**, *6*, 8488. [[CrossRef](#)] [[PubMed](#)]
128. Gabdulkhakov, A.; Guskov, A.; Broser, M.; Kern, J.; Müh, F.; Saenger, W.; Zouni, A. Probing the accessibility of the Mn₄Ca cluster in photosystem II: Channels calculation, noble gas derivatization, and cocrystallization with DMSO. *Structure* **2009**, *17*, 1223–1234. [[CrossRef](#)] [[PubMed](#)]
129. Linke, K.; Ho, F.M. Water in Photosystem II: Structural, functional and mechanistic considerations. *Biochim. Biophys. Acta* **2014**, *1837*, 14–32. [[CrossRef](#)]
130. Loll, B.; Kern, J.; Saenger, W.; Zouni, A.; Biesiadka, J. Towards complete cofactor arrangement in the 3.0 Å resolution structure of photosystem II. *Nature* **2005**, *438*, 1040–1044. [[CrossRef](#)] [[PubMed](#)]
131. Murray, J.W.; Barber, J. Structural characteristics of channels and pathways in photosystem II including the identification of an oxygen channel. *J. Struct. Biol.* **2007**, *159*, 228–237. [[CrossRef](#)]
132. Vassiliev, S.; Zaraiskaya, T.; Bruce, D. Exploring the energetics of water permeation in photosystem II by multiple steered molecular dynamics simulations. *Biochim. Biophys. Acta* **2012**, *1817*, 1671–1678. [[CrossRef](#)]
133. Wei, X.; Su, X.; Cao, P.; Liu, X.; Chang, W.; Li, M.; Zhang, X.; Liu, Z. Structure of spinach photosystem II–LHCII supercomplex at 3.2 Å resolution. *Nature* **2016**, *534*, 69–74. [[CrossRef](#)]
134. Sakashita, N.; Watanabe, H.C.; Ikeda, T.; Ishikita, H. Structurally conserved channels in cyanobacterial and plant photosystem II. *Photosynth. Res.* **2017**, *133*, 75–85. [[CrossRef](#)] [[PubMed](#)]
135. Sakashita, N.; Watanabe, H.C.; Ikeda, T.; Saito, K.; Ishikita, H. Origins of water molecules in the photosystem II crystal structure. *Biochemistry* **2017**, *56*, 3049–3057. [[CrossRef](#)] [[PubMed](#)]
136. Bommer, M.; Bondar, A.-N.; Zouni, A.; Dobbek, H.; Dau, H. Crystallographic and computational analysis of the barrel part of the PsbO protein of photosystem II: Carboxylate–water clusters as putative proton transfer relays and structural switches. *Biochemistry* **2016**, *55*, 4626–4635. [[CrossRef](#)] [[PubMed](#)]
137. Ono, T.; Zimmermann, J.L.; Inoue, Y.; Rutherford, A.W. EPR evidence for a modified S-state transition in chloride-depleted Photosystem II. *Biochim. Biophys. Acta* **1986**, *851*, 193–201. [[CrossRef](#)]
138. Amin, M.; Pokhrel, R.; Brudvig, G.W.; Badawi, A.; Obayya, S.S.A. Effect of chloride depletion on the magnetic properties and the redox leveling of the oxygen-evolving complex in photosystem II. *J. Phys. Chem. B* **2016**, *120*, 4243–4248. [[CrossRef](#)] [[PubMed](#)]
139. Rivalta, I.; Amin, M.; Lubner, S.; Vassiliev, S.; Pokhrel, R.; Umena, Y.; Kawakami, K.; Shen, J.-R.; Kamiya, N.; Bruce, D.; et al. Structural–functional role of chloride in photosystem II. *Biochemistry* **2011**, *50*, 6312–6315. [[CrossRef](#)] [[PubMed](#)]
140. Bricker, T.M.; Mummadisetti, M.P.; Frankel, L.K. Recent advances in the use of mass spectrometry to examine structure/function relationships in photosystem II. *J. Photochem. Photobiol. B* **2015**, *152*, 227–246. [[CrossRef](#)]
141. Weisz, D.A.; Gross, M.L.; Pakrasi, H.B. The use of advanced mass spectrometry to dissect the life-cycle of photosystem II. *Front. Plant Sci.* **2016**, *7*, 617. [[CrossRef](#)]
142. Weisz, D.A.; Gross, M.L.; Pakrasi, H.B. Reactive oxygen species leave a damage trail that reveals water channels in Photosystem II. *Sci. Adv.* **2017**, *3*, eaao3013. [[CrossRef](#)]
143. Dilbeck, P.L.; Bao, H.; Neveu, C.L.; Burnap, R.L. Perturbing the water cavity surrounding the manganese cluster by mutating the residue D1-Valine 185 has a strong effect on the water oxidation mechanism of photosystem II. *Biochemistry* **2013**, *52*, 6824–6833. [[CrossRef](#)]
144. Debus, R.J. Evidence from FTIR difference spectroscopy that D1-Asp61 influences the water reactions of the oxygen-evolving Mn₄CaO₅ cluster of photosystem II. *Biochemistry* **2014**, *53*, 2941–2955. [[CrossRef](#)] [[PubMed](#)]
145. Pokhrel, R.; Service, R.J.; Debus, R.J.; Brudvig, G.W. Mutation of lysine 317 in the D2 subunit of photosystem II alters chloride binding and proton transport. *Biochemistry* **2013**, *52*, 4758–4773. [[CrossRef](#)] [[PubMed](#)]
146. Wikström, M.; Sharma, V.; Kaila, V.R.I.; Hosler, J.P.; Hummer, G. New perspectives on proton pumping in cellular respiration. *Chem. Rev.* **2015**, *115*, 2196–2221. [[CrossRef](#)] [[PubMed](#)]
147. Konstantinov, A.A.; Siletsky, S.; Mitchell, D.; Kaulen, A.; Gennis, R.B. The roles of the two proton input channels in cytochrome c oxidase from *Rhodobacter sphaeroides* probed by the effects of site-directed mutations on time-resolved electrogenic intraprotein proton transfer. *Proc. Natl. Acad. Sci. USA* **1997**, *94*, 9085–9090. [[CrossRef](#)] [[PubMed](#)]

148. Wikström, M.; Jasaitis, A.; Backgren, C.; Puustinen, A.; Verkhovskiy, M.I. The role of the D- and K-pathways of proton transfer in the function of the haem-copper oxidases. *Biochim. Biophys. Acta* **2000**, *1459*, 514–520. [[CrossRef](#)]
149. Wikström, M.; Verkhovskiy, M.I. The D-channel of cytochrome oxidase: An alternative view. *Biochim. Biophys. Acta* **2011**, *1807*, 1273–1278. [[CrossRef](#)] [[PubMed](#)]
150. Popović, D.M.; Stuchebrukhov, A.A. Proton exit channels in bovine cytochrome c oxidase. *J. Phys. Chem. B* **2005**, *109*, 1999–2006. [[CrossRef](#)]
151. Tsukihara, T.; Aoyama, H.; Yamashita, E.; Tomizaki, T.; Yamaguchi, H.; Shinzawa-Itoh, K.; Nakashima, R.; Yaono, R.; Yoshikawa, S. The whole structure of the 13-subunit oxidized cytochrome c oxidase at 2.8 Å. *Science* **1996**, *272*, 1136–1144. [[CrossRef](#)]
152. Yoshikawa, S.; Muramoto, K.; Shinzawa-Itoh, K. The O₂ reduction and proton pumping gate mechanism of bovine heart cytochrome c oxidase. *Biochim. Biophys. Acta* **2011**, *1807*, 1279–1286. [[CrossRef](#)]
153. Lee, H.M.; Das, T.K.; Rousseau, D.L.; Mills, D.; Ferguson-Miller, S.; Gennis, R.B. Mutations in the putative H-channel in the cytochrome c oxidase from *Rhodobacter sphaeroides* show that this channel is not important for proton conduction but reveal modulation of the properties of heme a. *Biochemistry* **2000**, *39*, 2989–2996. [[CrossRef](#)]
154. Sharma, V.; Jambrina, P.G.; Kaukonen, M.; Rosta, E.; Rich, P.R. Insights into functions of the H channel of cytochrome c oxidase from atomistic molecular dynamics simulations. *Proc. Natl. Acad. Sci. USA* **2017**, *114*, E10339–E10348. [[CrossRef](#)] [[PubMed](#)]
155. Supekar, S.; Kaila, V.R.I. Dewetting transitions coupled to K-channel activation in cytochrome c oxidase. *Chem. Sci.* **2018**, *9*, 6703–6710. [[CrossRef](#)] [[PubMed](#)]
156. Liang, R.; Swanson, J.M.J.; Peng, Y.; Wikström, M.; Voth, G.A. Multiscale simulations reveal key features of the proton-pumping mechanism in cytochrome c oxidase. *Proc. Natl. Acad. Sci. USA* **2016**, *113*, 7420–7425. [[CrossRef](#)] [[PubMed](#)]
157. Wikström, M.; Verkhovskiy, M.I.; Hummer, G. Water-gated mechanism of proton translocation by cytochrome c oxidase. *Biochim. Biophys. Acta* **2003**, *1604*, 61–65. [[CrossRef](#)]
158. Wikström, M.; Krab, K.; Sharma, V. Oxygen Activation and Energy Conservation by Cytochrome c Oxidase. *Chem. Rev.* **2018**, *118*, 2469–2490. [[CrossRef](#)] [[PubMed](#)]
159. Busenlehner, L.S.; Salomonsson, L.; Brzezinski, P.; Armstrong, R.N. Mapping protein dynamics in catalytic intermediates of the redox-driven proton pump cytochrome c oxidase. *Proc. Natl. Acad. Sci. USA* **2006**, *103*, 15398–15403. [[CrossRef](#)] [[PubMed](#)]



© 2019 by the authors. Licensee MDPI, Basel, Switzerland. This article is an open access article distributed under the terms and conditions of the Creative Commons Attribution (CC BY) license (<http://creativecommons.org/licenses/by/4.0/>).